

Modular low noise readout method for a high-bandwidth MEMS force sensor

Jonas Valentijn, University of Twente, BSc-EE Thesis, August 8, 2022

Abstract—A method to read out a high-bandwidth force sensor using an instrumentation amplifier is presented. A sensor based on piezoresistive readout connected to a force sensing beam has been developed with a bandwidth of 75 kHz. With the goal to read out the force upon impact of tiny droplets of liquid to study needle-free injection methods. To read out the sensor, a method has been designed to take advantage of the high sensitivity and high-bandwidth. This method uses a modular PCB on which the sensor is attached. This gives the ability to quickly replace it. The high bandwidth is achieved with an amplifier with a bandwidth of 2.8 MHz. The measurement setup including, PCB, sensor and digitizer had an accuracy of 200 μN . With this new method multiple versions of the force sensor have been characterized. A maximum sensitivity of 1.669 N^{-1} is found and a maximum range of 13.5 mN. Comparing to previous results, a small improvement in sensor characteristics can be observed. In addition to this it can be used for other low force and high bandwidth measurement applications.

Index Terms—MEMS, force sensors, electric readout, high bandwidth, piezoelectric

I. INTRODUCTION

THE micro-electromechanical systems (MEMS) field of research is highly specialised, leading to a large range of applications. Force sensing is one of such applications where different specification, form-factors and methods are needed. A drawback of the designs being specialised meaning, each sensor needs custom readout hardware. Most MEMS designs however, are based on resistive or capacitive readout. Looking at some application for which MEMS based force sensors have been designed. A micro-force sensor to measure the flight force of a fruit fly [7]. An other more general design is a force-torque sensor based on capacitive readout [3]. A different interesting design that is able to change its resolution, sensitivity and bandwidth when applying a voltage to an adjustable-stiffness structure [5]. These sensors do have a lower bandwidth than 10 kHz which is common for force sensors [1]. A design focused on high frequency force sensing using a piezoresistive cantilever was designed. With this, it is possible to measure different small impacts. This cantilever approach resulted in a high bandwidth and resolution [4]. Trying to achieve both a high-bandwidth and sensitivity in a sensor, a high-bandwidth MEMS force sensor designed for the measuring of micro-jet injection has been designed [1]. To be able to read out the sensors, different methods were used. Due to the different specifications, the electric readout circuit has different requirements. The goal is to design a readout circuit to be able to fully use the high-bandwidth force sensor[1]. Using the designed readout circuit the force of a micro-droplet impact in time can be studied and be used in further research.

II. PREVIOUS WORK

A. Force sensor

To specify the requirements needed when designing the readout method. The applications and working principles of the sensor are of interest. The impact of a micro-droplet happens within 100 μs - 300 μs therefore a higher bandwidth is favourable increasing data samples [1]. Furthermore the impact force of needle-free drug delivery is in the order of milli newton [6]. These specifications lead to a design suited for this specific application. In figure 1 a schematic view of

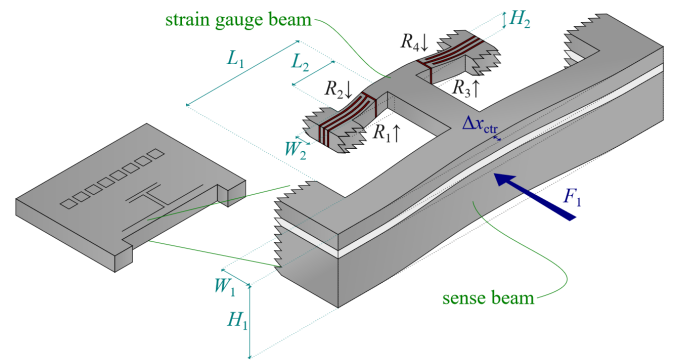


Fig. 1: Schematic view of the force sensor, showing the method on which it works. Applied force causes displacement putting strain on piezo resistors [1].

the high-bandwidth force sensor can be seen [1]. The design is based on two clamped beams rigidly connected with a center beam. A force can be applied to the larger beam, the stress and strain are mechanically amplified from the sensing beam to the strain gauge beam. The force causes a displacement in the beam, which is transferred by the center beam. This displacement creates a strain on the piezoresistive material. The strain gauges are in a Wheatstone bridge circuit to readout small changes in the electrical resistance caused by the strain. The difference in resistance can be observed by a changing output voltage, relative to the supply voltage as seen in equation 1.

$$V_{out} = \left(\frac{R_2}{R_1 + R_2} - \frac{R_3}{R_3 + R_4} \right) V_{sup} \quad (1)$$

In an ideal Wheatstone bridge, the output voltage should be zero when no force is applied. However, when fabricating the chip a difference in resistance is unavoidable. This is due to the method the piezoresistors are connected to the bonding pads. This can be seen in figure 2. Therefore, an unbalanced

Wheatstone bridge is used, meaning the output voltage will not be zero. The offset caused by this can be compensated for during the electric readout. The bandwidth of the sensor depends on its resonance frequency, which can be expressed as equation 2 [1].

$$f_0 = 6.48 \frac{W_1}{2\pi L_1^2 \sqrt{\frac{E}{\rho}}} \quad (2)$$

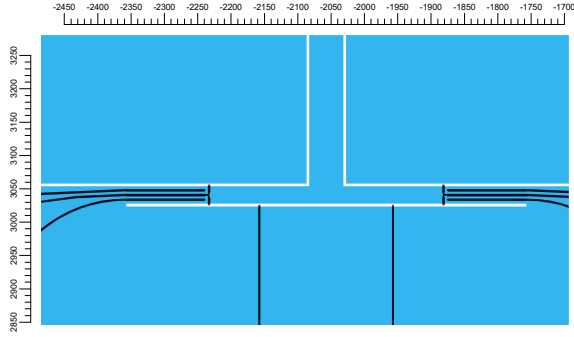


Fig. 2: Version 1 of the force sensor piezoresistor connection to mechanical force sensing beam and bonding pads.

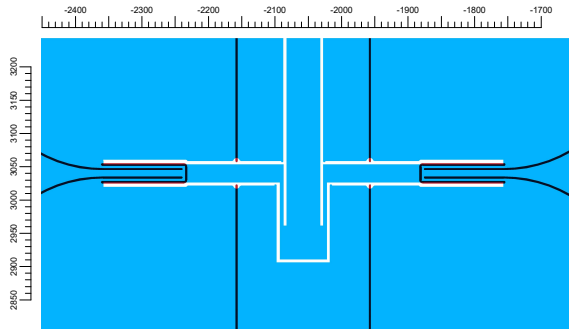


Fig. 3: Version 2 of the force sensor piezoresistor connection to mechanical force sensing beam, with changes to piezoresistor layout and mechanical connection.

Two versions of the force sensor have been developed. The changes made can be seen when comparing figure 2 and 3. In the second version, the middle piezoresistors have been merged, which means the piezoresistors are mechanically connected. This means the Wheatstone bridge is less unbalanced. Also, the mechanical connection has been changed to decrease the stiffness, this gives the possibility to decrease sensing beam size and increase bandwidth. Both improvements lead to an expected better performance of the force sensor.

Version 1 of the sensor has been characterized in the original paper, the results for sensitivity and bandwidth can be seen in table I and figure 4. During this measurement, a high linearity with a goodness of fit of $R^2 > 0.9999$ was found. A range of 13 mN was determined. To improve upon these measurements and use it for microsecond force measurements, a different readout method is needed since a lock-in amplifier has a long integration time. Which limits the bandwidth of the sensor.

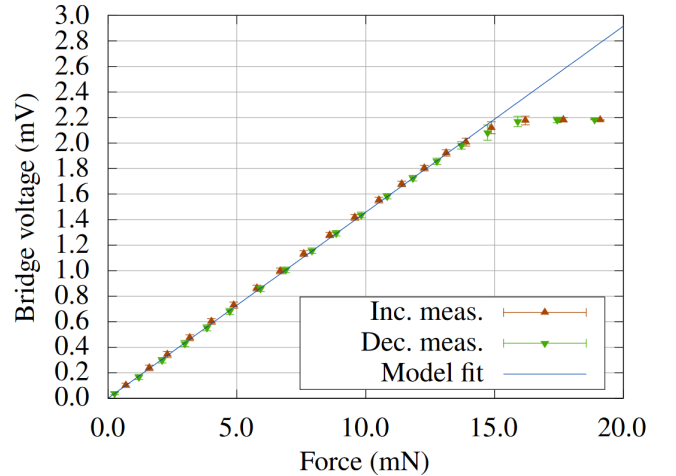


Fig. 4: Bridge voltage measurements found for increasing forces in millinewton range using a lock-in amplifier [1].

TABLE I: Theoretical, simulated and experimental values. For the sensitivity, and resonance frequency [1].

	Calculated	Simulated	Measured
$V_b/V_s F^{-1}$	$1.39 N^{-1}$	$1.34 N^{-1}$	$1.46 N^{-1}$
f_0	110 kHz	103 kHz	75 kHz

III. METHOD

A. Read-out circuit

The method to read out the Wheatstone bridge is based on the INA848, which is a low noise instrumentation amplifier. This instrumentation amplifier has a high bandwidth with a fixed gain of 2000. The instrumentation amplifier has a differential input with two buffer stages to negate having to match the impedance. The specific instrumentation amplifier that was chosen based on comparison between the needed requirements and availability of amplifiers. The INA848 offers other than a high gain also a bandwidth of 2.8 MHz and ultra-low noise of $1.5 \text{ nV}/\sqrt{\text{Hz}}$. This perfectly fits the requirements for the force sensor. Since the chosen instrumentation amplifier has a fixed gain of 2000 with a supply voltage between $\pm 15 \text{ V}$. The offset caused by the unbalanced Wheatstone bridge should not exceed this. To avoid this, the instrumentation amplifier has a built in voltage reference pin which can be used to tune the voltage down. This gives the ability to measure the force without the amplifier being clipped to its supply voltage. This also means the bridge voltage can be made higher while compensating for the increased output voltage caused by the offset. In figure 5 a simplified diagram of the instrumentation amplifier can be seen. The inputs of the instrumentation amplifier are the outputs of the Wheatstone bridge. From this, the relation between output voltage and inputs can be written as equation 3 [8]. This equation shows that the reference voltage can be added by applying a voltage. If the voltage needs to be negative or positive is determined by the way the Wheatstone bridge is connected.

$$V_{OUT} = 2000(V_{+IN} - V_{-IN}) + V_{ref} \quad (3)$$

To apply the reference voltage, an op-amp buffer stage with a resistive divider has been used. This resistive divider includes a

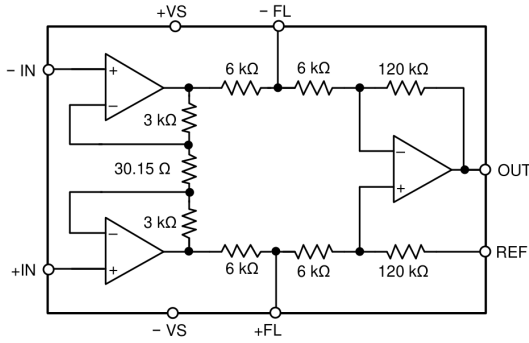


Fig. 5: Simplified diagram of the INA848 [8].

potentiometer. Which give the ability to change the reference voltage depending on which sensor is connected. To avoid noise from power supply affecting the performance of the instrumentation amplifier. Ultralow noise linear regulators are used, the same linear regulator is also used to drive the Wheatstone bridge voltage. To avoid unwanted behavior of two different linear regulators, two complementary linear regulators have been chosen. These linear regulators can be set at any voltage using the SET pin. This voltage is determined by a resistor and a current source at 100 μ A. Meaning a resistor at 1 % of wanted voltage should be used. The linear voltage regulators are LT3045 and LT3094 from Analog devices. A simulation using LTSpice has been done to check if the design gave the expected output.

B. PCB

The designed circuit used for measuring includes the components discussed previously. From this circuit, a PCB has been designed including, a PCIe x1 connector with 36 contacts, mounting holes and the output coax connector. A four layer PCB design is used, the output trace and supply trace are in the second and third layers between two ground layers, this helps shield against noise. The chips which are surface mounted are shielded using a RF shield. The data sheets are followed for good PCB practices and extra components are included in case different a supply voltage is wanted. To be able to measure the chip without the amplifier two extra coax connections are added directly to the sensor.

C. Modular breakout board for force sensor

To be able to test multiple chips, it is necessary to be able to change the chip effortlessly. To do this, the chip will be mounted on a separate board with a PCIe connector. Each chip has to be adhered to the breakout board and wire-bonded to the SMD pads. The Wheatstone bridge connections are made on the breakout board. Thus, the breakout board can directly plugged into main board. The breakout board is being mechanically strengthened by a separate 3D printed bracket.

D. Measurement setup

The measurement setup consists of three parts. A schematic overview of the measurement setup can be seen in figure 6.

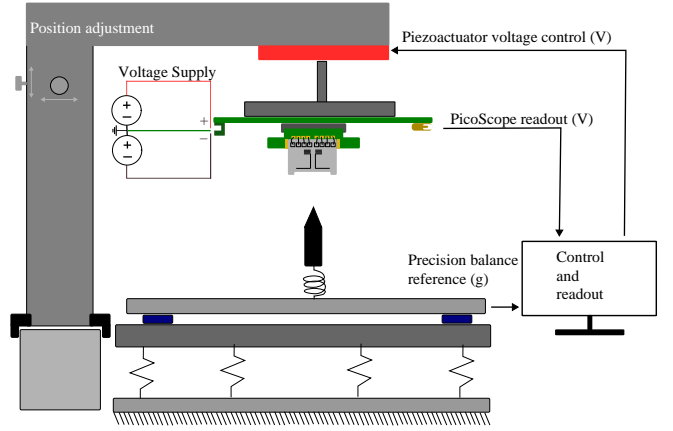


Fig. 6: Schematic overview of the used measurement setup to characterize the force sensor (front view).

The whole setup is build upon a table-top with tuned damping (Newport RS4000) on laminar flow isolators (Newport I-2000). The piezoelectric actuator (P-603.3S2) with a full range of 380 μ m is mounted to a metal frame. To this actuator, the PCB is connected using a metal bracket. On the PCB the force sensor is connected using a card-edge connector (PCIe). This force sensor is adhered to the breakout board using epoxy glue. The PCB will be lowered onto a small needle using the piezo actuator. This small needle is positioned on a precision balance (Mettler Toledo AT200) which is used to determine the force applied as a reference. To align the needle and force sensor, a microscope is used and a translation stage (Thorlabs MVS005/M). The output of this circuit is connected using a coaxial cable to the PicoScope 5024A. The PicoScope digitizes the analog output. To avoid quantisation noise and achieve the highest possible accuracy. The resolution of eight bits can be enhanced to get twelve effective number of bits using a moving average filter (low-pass filter). Using a lower range can also increase accuracy (more bits for smaller voltage) however, due to offset in piezoresistor a balance has to be found between range and the bridge supply voltage. It has been chosen to use a range of ± 10 V, This leads to a LSB of 4.88 mV, this negatively impacts the accuracy. The highest possible sample rate of the PicoScope at these settings is 9.615 MS/s. Each measurement is saved for a time period of 1 second, thus $9.615 \cdot 10^6$ samples will be averaged over to find the mean values and standard deviation. This data is saved using PicoScope 6 software and processed using MATLAB. The reference force data is saved using LabView at time interval of 1.5 s. The Piezo actuator can also be controlled using LabView and a GPIB to USB connector. A range of voltages is applied to the piezo actuator. To make sure small forces can be applied, an extra spring is added between the needle and the balance. This spring is a steel plate ($E=180$ GPa [9]) resting on two blocks as a double supported spring [2].

$$F = \Delta x k \quad (4)$$

To determine the force, Hooks' law can be used (Eq.4). In this equation F is the force in Newton, k is the spring constant in N/m^2 , and Δx is the displacement in meters. Filling the displacement for a double supported spring with rectangular moment of inertia and bending moment at $L/2$ [2]. Hooks' law can be written as equation 5. Where E is Young's modulus in Pascal, b the width in meters, h the height in meters and L the length in meters.

$$F = \Delta x \frac{4Ebh^3}{L^3} \quad (5)$$

Filling the dimensions, $L = 6$ cm, $b = 5$ mm, $h=1$ mm into the formula for a double supported spring (Eq.6).

$$k = \frac{4Ebh^3}{L^3} = 1.66 \cdot 10^4 \text{ [N}/\text{m}^2] \quad (6)$$

Due to the high spring constant, a small displacement is needed from the piezo actuator. To do this, small voltage steps are applied using a DC power supply (Agilent E3631A). Steps of 20 mV lead to a displacement of approximately 0.5 μm (max is 380 μm at 12 V). With this force in range of 0.5 mN can be applied. The force is increased linearly to find the expected linear relation between force and bridge voltage. This is done with steps of 10 mV and 20 mV. A spring with a lower spring constant for smaller force steps has been designed which could be 3D printed. However, due to possible drift in the material that could occur during measurements this has not been used. An alternative method to avoid this problem is to place the PCB on the balance. Although due to the cables coming from the PCB affecting the measurements of the small forces, this is not a solution.

IV. RESULTS AND DISCUSSION

A. INA848

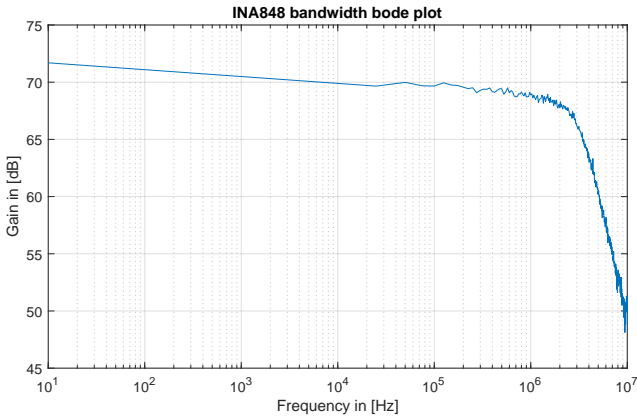


Fig. 7: Gain plot of INA848 at a input voltage 200 μV .

To check if the INA848 behaves similar to its data sheet. The gain and phase were analysed for a frequency up to 10 MHz. This was done using the HP 4194A Gain/Phase Analyzer. The bandwidth in figure 7 is at 2.8 MHz which is the specified bandwidth in the data sheet. It can be seen that this point lays at around -3dB which was expected. The gain is between 72 and 66 dB between 0-2.8 MHz which is higher than the

specified 2000 gain. This is caused by the low amount of measurement points in the lower frequencies. From the point of 2.8 MHz the roll-off is 33.52 dB/decade. There is a phase shift of -129 deg at 2.8 MHz. There is a -180 deg phase shift at 4 MHz which converges back to 0 deg. The time delay of the amplifier increases slightly at higher frequencies. At 2.8 MHz the time delay is 9.84 ns.

B. Characterization force sensor version 1

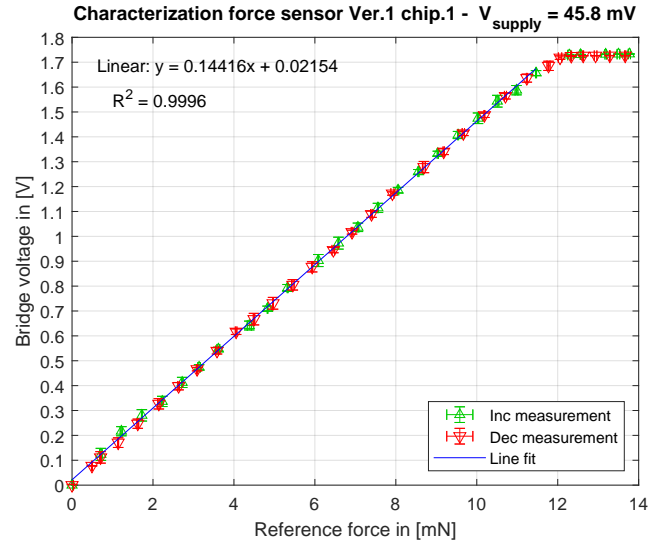


Fig. 8: Version 1 chip 1. Bridge voltage measured (offset corrected) for increasing and decreasing reference forces, including the line fit and standard deviation for bridge voltage and reference force.

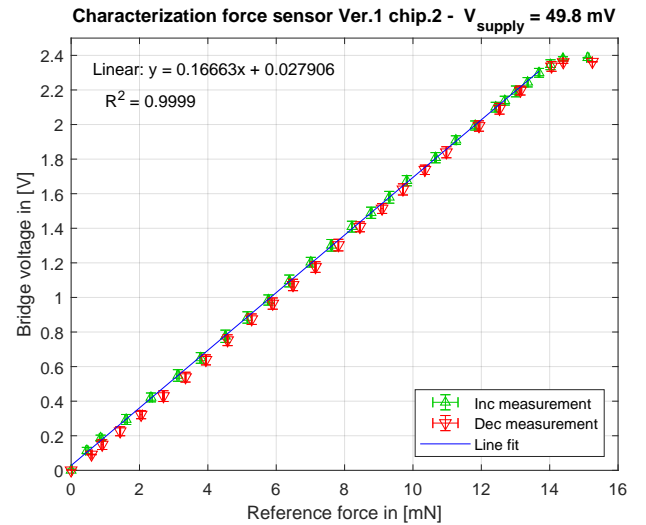


Fig. 9: Version 1 chip 2. Bridge voltage measured (offset corrected) for increasing and decreasing reference forces, including the line fit and standard deviation for bridge voltage and reference force.

Multiple different force sensors have been measured at different supply voltages. This is due to difference in Wheatstone bridge offset, the maximum possible supply voltage has been

applied with the output of the amplifier within 10 V range while using the -15 V reference pin of the instrumentation amplifier. This gave a supply voltage close to 50 mV for version 1 of the sensor. Meaning maximum resistive offset at 50 mV is approximately between 10-12.5 mV (25%) and with amplification 20-25 V. Multiple measurements for each chip have been done, this resulted in the following results in figure 8 and 9 for chip 1 and 2 respectively.

It can be noted that in both figures 8 and 9 that the standard deviation is much higher within the range of sensor. This standard deviation is on average 30 mV. This leads to accuracy of 180-200 μN . Thus, other than the noise of the circuit and quantisation, the sensor itself also contributes noise to the measurement. From table II the sensitivity and range found from the chips. Using a chip with a lower Wheatstone bridge offset could improve the accuracy.

TABLE II: Sensitivity and range for version 1 adjusted for gain of amplifier.

	Ver.1 Chip.1	Ver.1 Chip 2
Sensitivity ($V_b/V_s F^{-1}$)	$1.573N^{-1}$	$1.669N^{-1}$
Range	12.5 mN	13.5 mN

C. Characterization force sensor version 2

When characterizing the second version of the force sensor, three different chips were tested. The same method was used as for version 1 of the sensor. Two of the three gave no change in bridge voltage when applying a force. It was noted that during the manufacturing of the chips, some piezoresistors were not completely etched through. This is likely the cause of the sensors not working. The third chip that was tested did give a change in bridge voltage, from the measurements however no clear linear relation was observed. Also, the difference in bridge voltage was much lower compared to version 1. The chip was only measured once, thus no meaningful conclusion can be made. To properly test the second version, more chips must be tested or a new manufacturing run of the chip must be done.

D. Comparison to previous work

Comparing the range of the two chips and the one measured in the original paper. It can be observed that the range for between these sensors had a deviation of around 0.5 mN and a 13 mN range cannot be guaranteed. Furthermore, the sensitivity of both chips measured is higher than the originally found $1.46 N^{-1}$. Comparing both readout methods, the lock-in amplifier has a higher accuracy of 100 μN [1], this is due to long the integration time. For this reason however, it cannot be used for high bandwidth measurements. The developed method has a lower accuracy at 200 μN with a much higher bandwidth (2.8 MHz). Comparing the accuracy, the new method has 100 μN worse accuracy. The sensor has a bandwidth of 75 MHz this is well below the bandwidth of the INA848 meaning to full bandwidth of the sensor can be utilised.

V. CONCLUSION

A method to read out a high-bandwidth force sensor using instrumentation amplifier has been designed. The designed method has been tested, characterizing multiple force sensor chips. From this, it was found out that the force sensor has a higher sensitivity than previously measured with a highest sensitivity of $1.669 N^{-1}$. This was measured with an accuracy of 200 μN . The designed readout method gives the ability to quickly replace different force sensors without the need to solder components, furthermore it gives the ability to use the full bandwidth of the force sensor. Meaning that both the sensitivity and bandwidth of this sensor can be fully utilised. This makes it possible to measure the impact in a range of 10 microseconds, which can be beneficial when studying liquids. For future work the readout method can be tested with microsecond impacts for which it was designed. Also, the second version of the force sensor can be tested.

REFERENCES

- [1] Dennis Alveringh et al. "Miniature Robust High-Bandwidth Force Sensor with Mechanically Amplified Piezoresistive Readout". In: *IEEE Symposium on Mass Storage Systems and Technologies* 2022-January (2022), pp. 684–687. ISSN: 21601968. DOI: 10.1109/MEMS51670.2022.9699639.
- [2] *Beams - Supported at Both Ends - Continuous and Point Loads*. URL: https://www.engineeringtoolbox.com/beam-stress-deflection-d_1312.html.
- [3] Felix Beyeler, Simon Muntwyler, and Bradley J. Nelson. "A six-axis MEMS force-torque sensor with micro-Newton and nano-Newtonmeter resolution". In: *Journal of Microelectromechanical Systems* 18.2 (2009), pp. 433–441. ISSN: 10577157. DOI: 10.1109/JMEMS.2009.2013387.
- [4] J. C. Doll et al. "High frequency force sensing with piezoresistive cantilevers". In: *TRANSDUCERS 2009 - 15th International Conference on Solid-State Sensors, Actuators and Microsystems* (2009), pp. 1928–1931. DOI: 10.1109/SENSOR.2009.5285696.
- [5] Mohammad Maroufi et al. "An adjustable-stiffness MEMS force sensor: Design, characterization, and control". In: *Mechatronics* 56 (Dec. 2018), pp. 198–210. ISSN: 09574158. DOI: 10.1016/J.MECHATRONICS.2018.05.007. URL: <https://doi.org/10.1016/j.mechatronics.2018.05.007>.
- [6] Jeanne C. Stachowiak et al. "Piezoelectric control of needle-free transdermal drug delivery". In: *Journal of Controlled Release* 124.1-2 (Dec. 2007), pp. 88–97. ISSN: 01683659. DOI: 10.1016/J.JCONREL.2007.08.017. URL: www.elsevier.com/locate/jconrel.
- [7] Yu Sun et al. "Drosophila flight force measurements using a MEMS micro force sensor". In: *Annual International Conference of the IEEE Engineering in Medicine and Biology - Proceedings* 26 III (2004), pp. 2014–2017. ISSN: 05891019. DOI: 10.1109/IEMBS.2004.1403593.
- [8] Texas Instruments. "INA848 Ultra-Low-Noise (1.5 nV/ $\sqrt{\text{Hz}}$), High-Bandwidth Instrumentation Amplifier With Fixed Gain of 2000 1 Features". In: (2020). URL: <https://www.ti.com/lit/ds/symlink/ina848.pdf?ts=1653999671213>.
- [9] *Young's Modulus, Tensile Strength and Yield Strength Values for some Materials*. URL: https://www.engineeringtoolbox.com/young-modulus-d_417.html.

APPENDIX A SIMULATION READOUT CIRCUIT

Simulation results of the complete circuit for different resistances can be seen in table III. The values used and connections made for each IC can be seen in figure 10.

TABLE III: Simulation results for different resistances at Wheatstone bridge

R1 & R4	R2 & R3	V_{out}
300 Ω	180 Ω	10.40 V
305 Ω	175 Ω	12.48 V
305 Ω	170 Ω	13.82 V

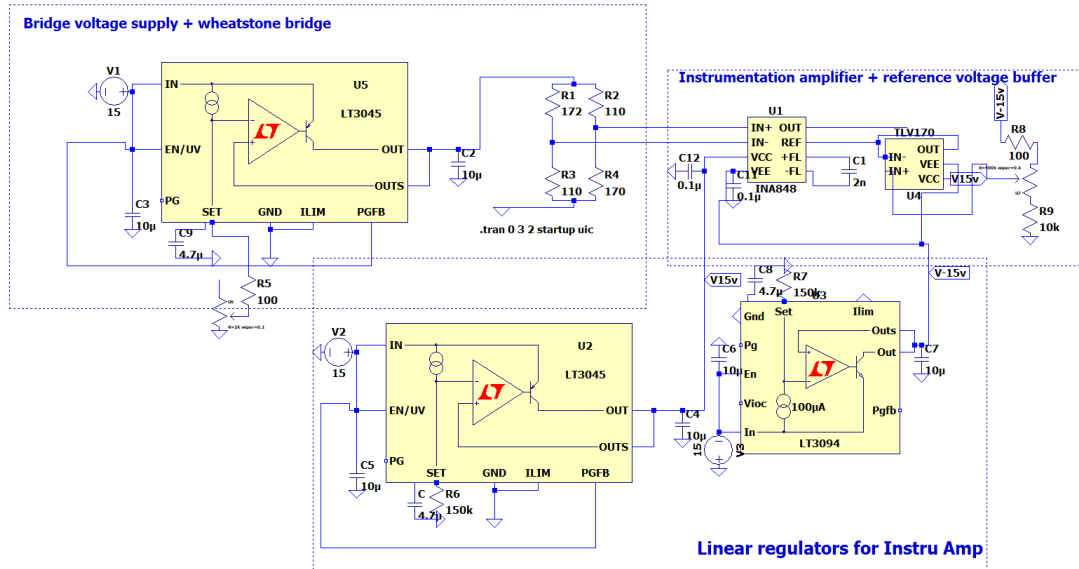


Fig. 10: LTspice implementation using the ICs used in the actual circuit

APPENDIX B SCHEMATIC CIRCUIT AND PCB LAYOUT OF THE READOUT CIRCUIT

The schematic used for creating the PCB is made with EAGLE and can be seen in figure 11. This schematic is exported into a PCB file, the PCB layout with all traces can be seen in figure 12. The dimensions of the PCB is 8.5 cm by 8.5 cm. Mounting holes for the aluminium PCB holder are specified in the figure. The modular breakout board with copper pad onto which the force sensor can be adhered to can be seen in figure 13. This figure also included the SMD pads for wire bonding and the connections made for the Wheatstone bridge.

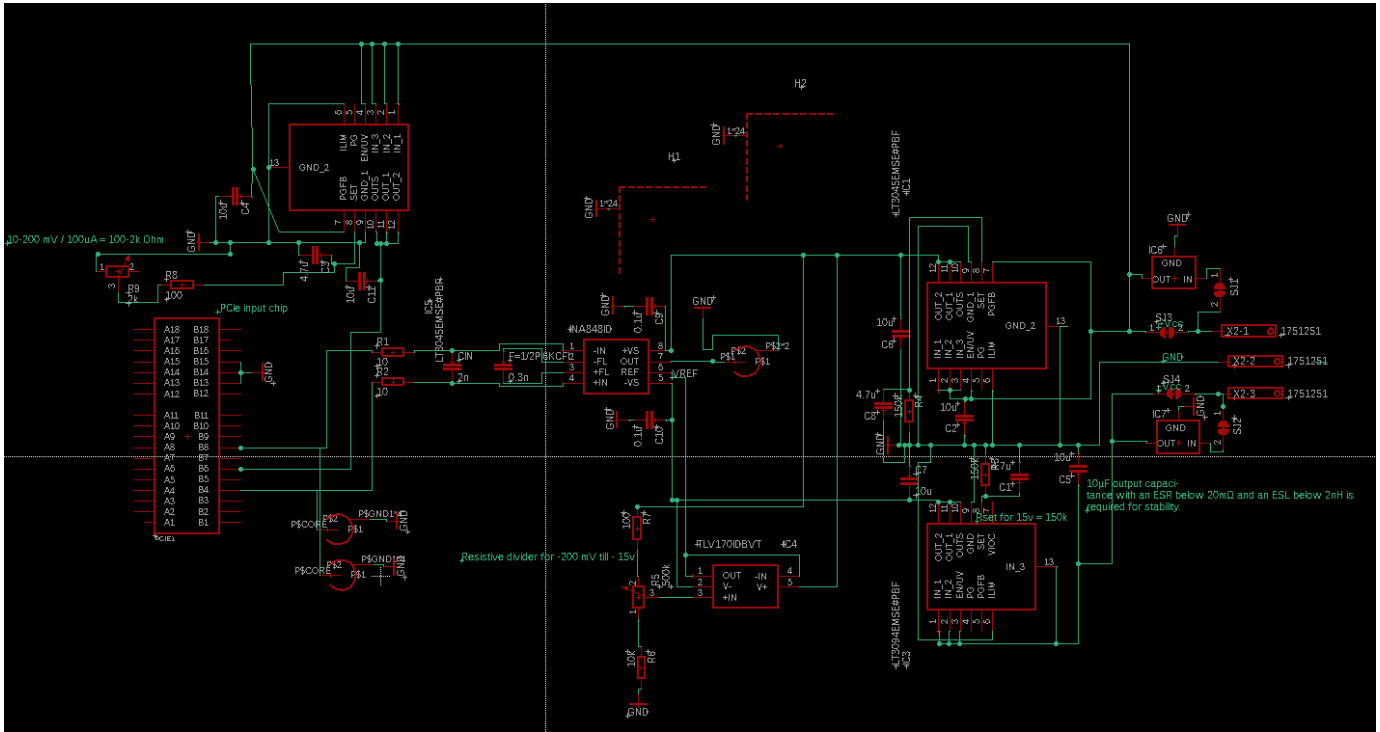


Fig. 11: Schematic of all the connectors and ICs for creating PCB (EAGLE)

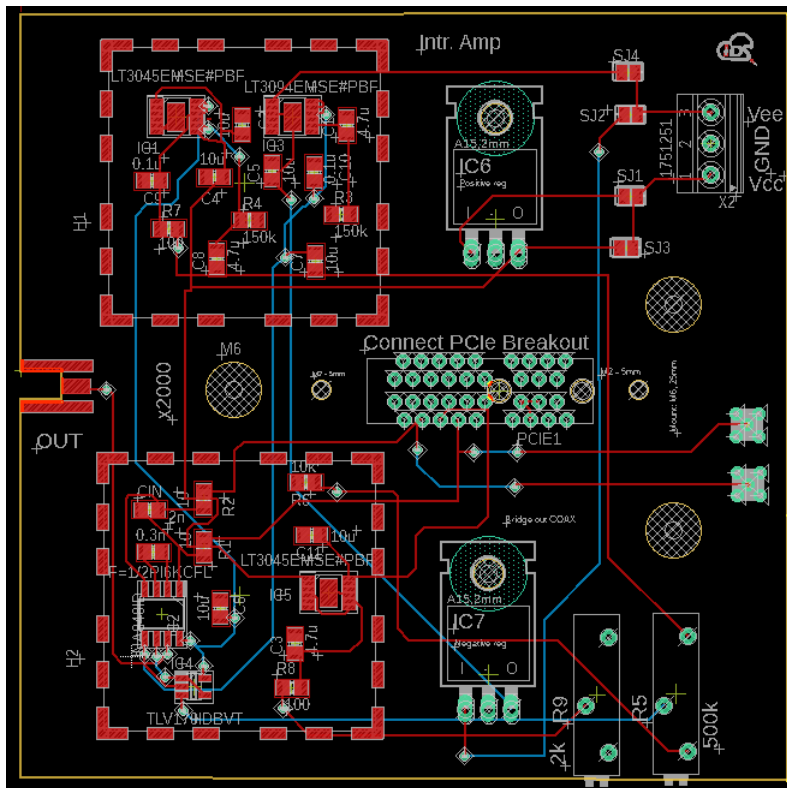


Fig. 12: PCB implementation in EAGLE using 4 layers, with output and supply in layer 2,3

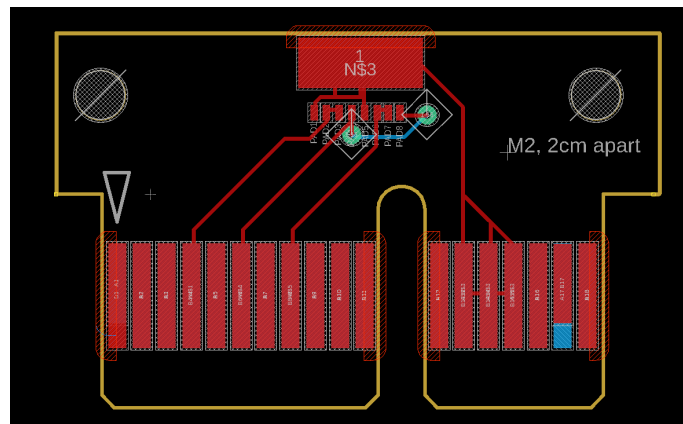
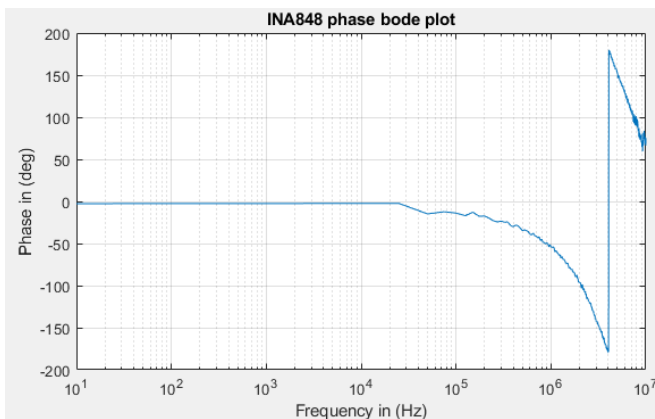


Fig. 13: Breakout PCB board layout, including pads for sensor and easy wirebonding layout

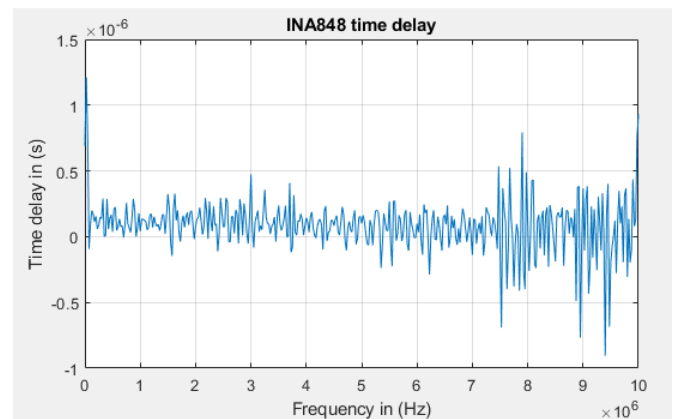
APPENDIX C

INA848 PHASE AND TIME DELAY

The figure 14 shows the phase and time delay measured using the gain/phase analyzer specified in the paper.



((a)) Phase of the INA848 for 10-10MHz



((b)) Time delay of the INA848 for 10-10MHz

Fig. 14: INA848 measurements of the phase and the time delay

APPENDIX D
ASSEMBLED PCB AND MEASUREMENT SETUP

The previous shown PCB and components have been ordered and fully assembled. Figure 15 shows the completed PCB including the RF shields and the 3D brackets to strengthened the breakout PCB with force sensor. The PCB mounted upside down to the piezoactuator can be seen in figure 16. Underneath the PCB the spring and needle can be seen on the balance. The needle is precisely positioned using the microscope on the right and the translation stage on the left.

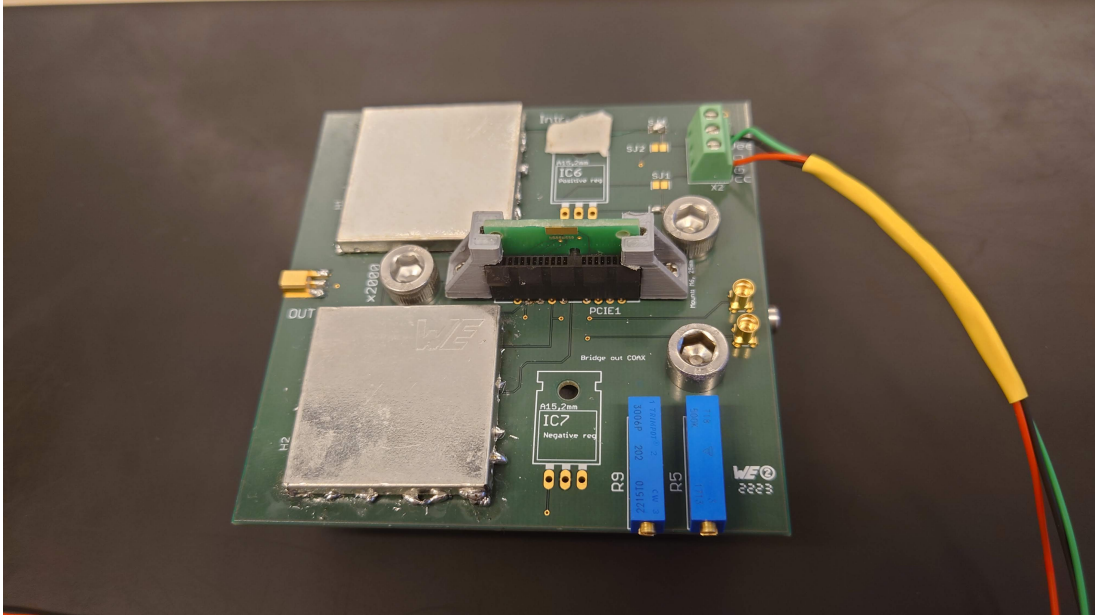


Fig. 15: Fully assembled PCB, including all components and 3D printed bracket.

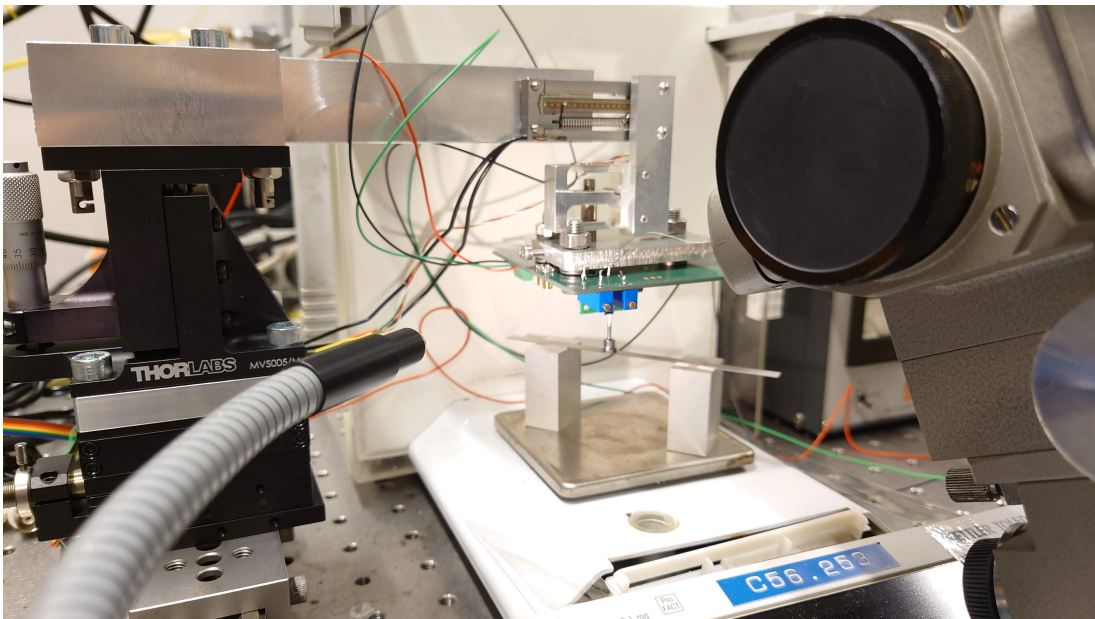


Fig. 16: Picture of measurement setup during on of the measurments

APPENDIX E
3D MODELS AND SPRING CONSTANT CALCULATION

For the designed spring that was mentioned in the paper, the spring consist of three connected double beams. The spring constant for this can be written as equation 7. Filling in the dimensions of springs, $L = 2 \text{ mm}$, $b = 1 \text{ cm}$, $h = 300 \text{ }\mu\text{m}$ results in a spring constant of 81 N/m^2

$$k = \frac{3}{2} \frac{Eh^3L}{b^3} = 81 \text{ N/m}^2 \quad (7)$$

The 3D model using these dimensions and three springs can be seen in figure 17. The 3D model of the aluminium bracket to hold the PCB upside down above the balance can be seen in figure 18 the dimensions are 5 cm by 2.5 cm. A screw is screwed in from the side to secure the metal rod to the bracket. The bracket to strengthened the breakout PCB is made to perfectly fit the PCIe 1x connector. This can be seen in figure 19 which also includes the PCIe connector.

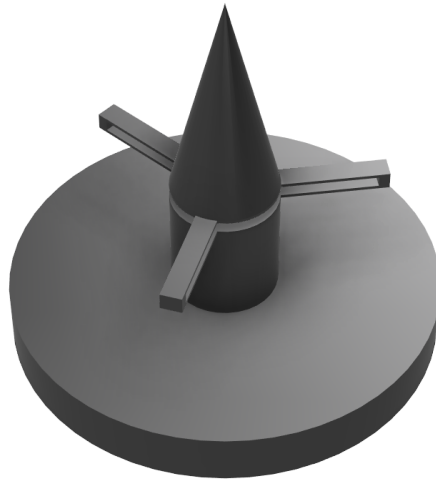


Fig. 17: Custom spring needle combo design



Fig. 18: 3D model of aluminum PCB holder

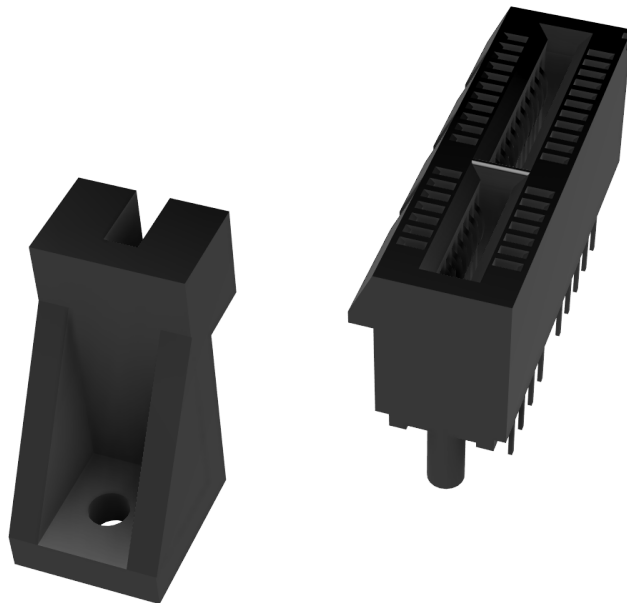
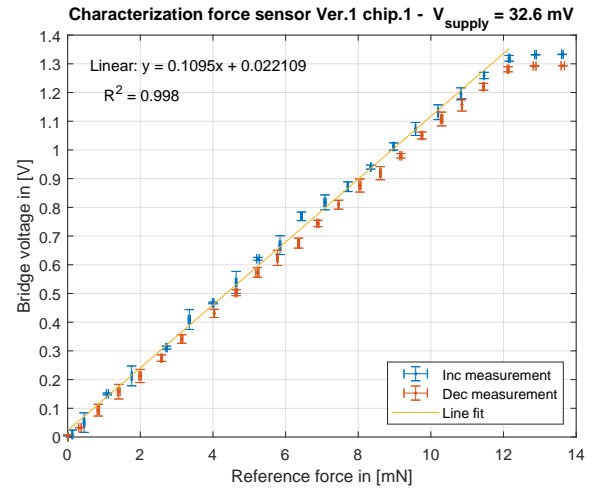
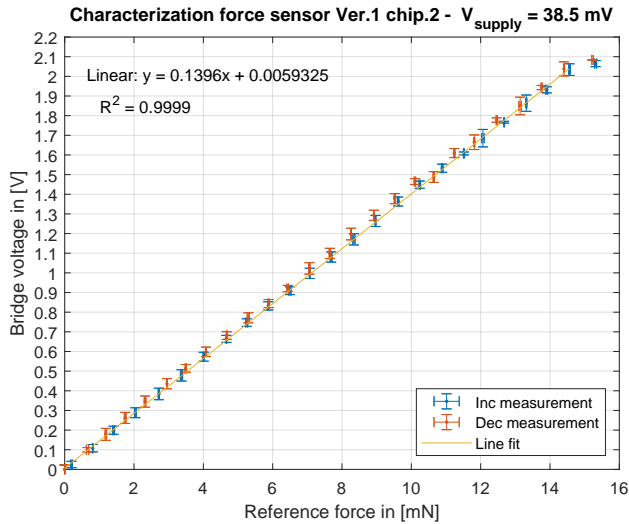


Fig. 19: Bracket to hold the PCB breakout

APPENDIX F
MEASUREMENTS DONE WITH CHANGES IN SETUP

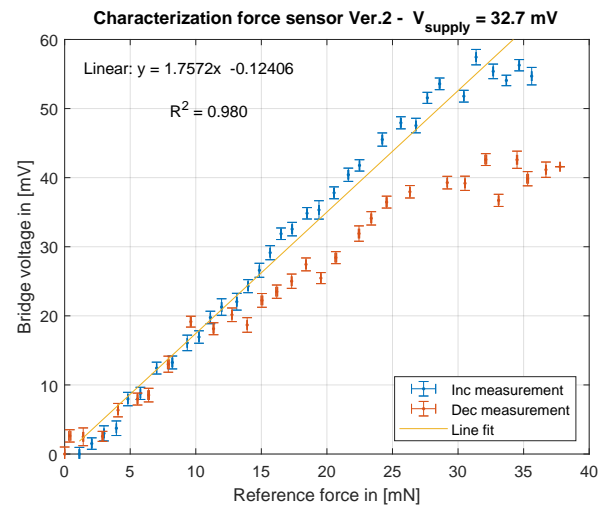
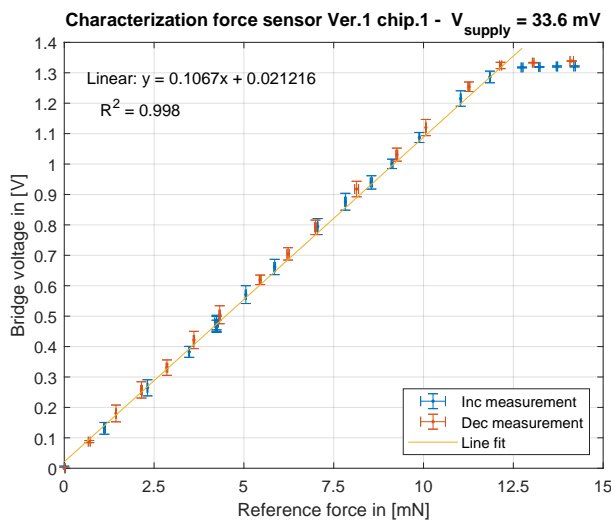
In addition to the measurement results shown in the paper, many more measurements were done. Measurements on version 1 with the second PCB are shown in figure 20(a) & 20(b), these results show similar results to those in the paper. In figure 21(a) & 21(b) one more measurement for version 1 chip 1 is shown and also the measurement of second version of the chip. The measurement of version 2 does show some linearity. But as explained in the paper has a much higher range and much lower voltage difference for similar forces as version 1, which is not expected. Since the chip broke after the first measurement there was no option to measure it again. In figure 22(a) & 22(b) two measurements were done using the first PCB which had noise due to the linear regulars oscillating. Finally in table IV all the sensitivities and ranges for all different measurements are listed.



((a)) Version 1 chip 2 at supply of 38.6 mV. Bridge voltage measured (offset corrected) for increasing and decreasing references forces, including the line fit and standard deviation for bridge voltage and reference force.

((b)) Version 1 chip 1 at supply of 32.6 mV. Bridge voltage measured (offset corrected) for increasing and decreasing references forces, including the line fit and standard deviation for bridge voltage and reference force

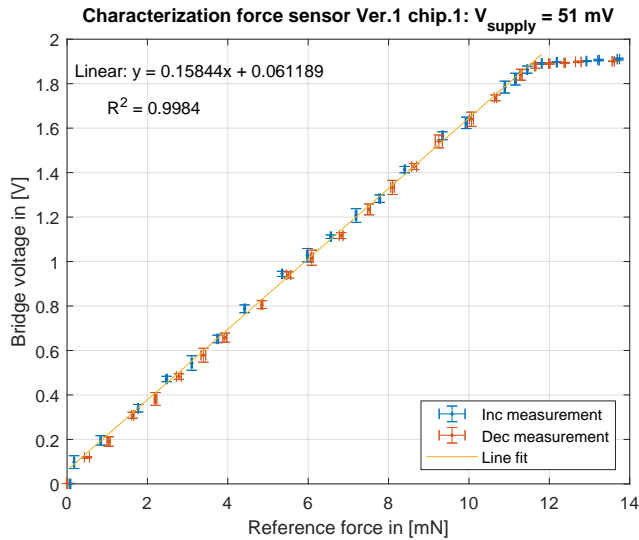
Fig. 20: Chip 1 and 2 (version 1) measured with same setups



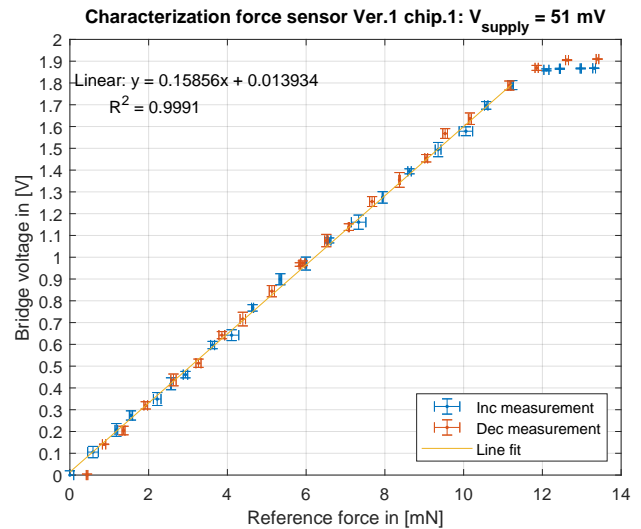
((a)) Version 1 chip 1 at supply of 33.6 mV. Bridge voltage measured (offset corrected) for increasing and decreasing references forces, including the line fit and standard deviation for bridge voltage and reference force

((b)) Version 2 at supply of 32.7 mV. Bridge voltage measured (offset corrected) for increasing and decreasing references forces, including the line fit and standard deviation for bridge voltage and reference force

Fig. 21: In figure 21(a) another measurement of chip 1 version 1. In figure 21(b) the second version is measured using first PCB with applied low-pass filter



((a)) Version 1 chip 1 at supply of 51 mV. Bridge voltage measured (offset corrected) for increasing and decreasing reference forces, including the line fit and standard deviation for bridge voltage and reference force



((b)) Version 1 chip 1 at supply of 51 mV. Bridge voltage measured (offset corrected) for increasing and decreasing reference forces, including the line fit and standard deviation for bridge voltage and reference force

Fig. 22: Both these measurements were done using version of the PCB where the linear regulator was oscillating and a low-pass filter was used to correct this.

TABLE IV: Sensitivity and range for all the figures adjusted for gain of amplifier

Figure	20(a)	20(b)	21(a)	21(b)	22(a)	22(b)
Sensitivity ($V_b/V_s F^{-1}$)	$1.812N^{-1}$	$1.679N^{-1}$	$1.587N^{-1}$	$0.026N^{-1}$	$1.552N^{-1}$	$1.553N^{-1}$
Range	13.5 mN	12.5 mN	12.5 mN	30 mN	12.5 mN	12.5 mN